

Dataset of artefacts for machine learning applications in astronomy

Sreevarsha Sreejith^a, Maria V. Pruzhinskaya^{b,c}, Alina A. Volnova^d, Vadim V. Krushinsky^e, Konstantin L. Malanchev^f, Emille E. O. Ishida^c, Anastasia D. Lavrukhina^b, Timofey A. Semenikhin^{b,g}, Emmanuel Gangler^c, Matwey V. Kornilov^{b,h}, Vladimir S. Korolevⁱ

^aPhysics Department, University of Surrey, Stag Hill Campus, Guildford, GU2 7XH, Surrey, UK

^bLomonosov Moscow State University, Sternberg Astronomical Institute, Universitetsky pr. 13, Moscow, 119234, Russia

^cUniversite Clermont Auvergne, CNRS, LPCA, Clermont-Ferrand, F-63000, France

^dSpace Research Institute of the Russian Academy of Sciences (IKI), 84/32 Profsoyuznaya Street, Moscow, 117997, Russia

^eLaboratory of Astrochemical Research, Ural Federal University, Ekaterinburg, ul. Mira d. 19, Yekaterinburg, 620002, Russia

^fMcWilliams Center for Cosmology & Astrophysics, Department of Physics, Carnegie Mellon University, Philadelphia, PA 15213, USA

^gLomonosov Moscow State University, Faculty of Physics, Leninskie Gory 1-2, Moscow, 119991, Russia

^hNational Research University Higher School of Economics, 21/4 Staraya Basmanaya Ulitsa, Moscow, 105066, Russia

ⁱIndependent researcher

Abstract

Accurate photometry in astronomical surveys is challenged by image artefacts, which affect measurements and degrade data quality. Due to the large amount of available data, this task is increasingly handled using machine learning algorithms, which often require a labelled training set to learn data patterns. We present an expert-labelled dataset of 1127 artefacts with 1213 labels from 26 fields in ZTF DR3, along with a complementary set of nominal objects. The artefact dataset was compiled using the active anomaly detection algorithm PINEFOREST, developed by the SNAD team. These datasets can serve as valuable resources for real-bogus classification, catalogue cleaning, anomaly detection, and educational purposes. Both artefacts and nominal images are provided in FITS format in two sizes (28×28 and 63×63 pixels). The datasets are publicly available for further scientific applications.

Keywords: artefacts, image analysis, classification, sky surveys

1. Introduction

With the advent of existing wide-field surveys like the Zwicky Transient Facility (ZTF, Bellm et al. 2019), the Euclid Mission (Refregier et al., 2010) and the James Webb Space Telescope (Gardner et al., 2006) and upcoming surveys such as the Vera C. Rubin Observatory Legacy Survey of Space and Time (LSST, Ivezić et al. 2019), preparing astronomical data for human analysis has become an increasingly challenging task. Since the amount of data makes individual object inspection prohibitive, this is achieved through efficient algorithms and high performance computing, often incorporating machine learning techniques. Most surveys have an initial filter that removes objects or features that are deemed spurious in images and catalogs as part of their data processing pipeline (e.g., Kornilov et al. 2012; Duev et al. 2019). However, this step is not entirely foolproof, leaving artefacts such as reflection ghosts, bad columns, satellite tracks, as well as photometric contamination of real objects due to light from nearby bright stars or closely passing asteroids (e.g. Malanchev et al., 2021; Sánchez-Sáez et al., 2021; Pruzhinskaya et al., 2023). These artefacts can appear in some exposures and disappear in others, affecting astrometric calibration and the photometry of nearby objects, ultimately degrading data quality. Thus, their identification and removal are of paramount importance before the compilation of science-ready catalogs.

There has been some limited effort to detect and/or mask artefacts in images, focusing on data from different surveys such as Desai et al. (2016), Chang et al. (2021) and Tanoglidis et al. (2022). However, most of the related work uses statistical/deep learning algorithms to classify objects into ‘real’ or ‘bogus’ such as Duev et al. 2019; Paranjpye et al. 2019; Carrasco-Davis et al. 2021; Killestein et al. 2021; Semenikhin et al. 2024; Weston et al. 2024. A common requirement for this approach is a labeled dataset for classifier training, which is not always easy to obtain. While image artefacts can be simulated (e.g., Pöntinen et al. 2023), visual inspection of real data remains the most direct way to obtain accurate labels. However, labeling is a time-consuming and resource-intensive process. In recent years, this task has been partially delegated to citizen science initiatives such as Zooniverse¹ (formerly Galaxy Zoo), its transient-specific branch Zwickyverse², the Jupiter-specific project Jovian Vortex Hunter (Sankar et al., 2024), and others. While citizen science projects can produce large amounts of labelled data, this will generally be accompanied by large uncertainties requiring careful statistical modelling before their results can be used in subsequent studies. Labels provided by astronomers – though fewer – are likely to be more accu-

¹<https://www.zooniverse.org/>

²<https://www.zooniverse.org/projects/rswcit/zwickys-quirky-transients>

rate and thus better suited as input for machine learning algorithms. Moreover, experts can identify the most probable cause for a given artefact, thus also contributing to the diagnostic and improvement of instrument operations. Even a relatively small data set, compiled by experts, can be a valuable starting point for machine learning algorithms. For example, Semenikhin et al. 2024 demonstrated that high real-bogus classification performance can be achieved starting from just over 3000 expert-labelled examples for training. Thus, the goal of this work is to provide expert-labeled datasets of both artefacts and non-artefacts (hereafter referred to as nominals) from the ZTF survey. These datasets can be used for scientific tasks such as real-bogus classification and anomaly detection, as well as for education and outreach.

Since 2018, the SNAD³(Volnova et al., 2024) team has been working on different aspects of anomaly detection in astrophysical data, leading to the development of the *coniferest*⁴ package (Kornilov et al., 2024), which incorporates several anomaly detection algorithms, including ISOLATION FOREST (Liu et al., 2008), ACTIVE ANOMALY DISCOVERY (Das et al., 2017; Ishida et al., 2021), and PINEFOREST (Korolev et al., in prep.). These algorithms have been applied to studies of transients and variable objects, including supernovae, variable stars, and red dwarf flares (Pruzhinskaya et al., 2019; Malanchev et al., 2021; Pruzhinskaya et al., 2023; Voloshina et al., 2024). The SNAD team’s efforts have also resulted in the creation of the SNAD anomaly knowledge base (Malanchev et al., 2023), which provides labels for thousands of ZTF objects, which, in turn, has been the motivation for this work.

This paper is organised as follows. Section 2 describes the data selection process. Section 3 defines the labels used in this work according to the SNAD labelling schema. Section 4 details the algorithm and its implementation. Sections 5-6 present the results and their discussion, respectively. Section 7 provides a summary and conclusions.

2. Data

The Zwicky Transient Facility is a wide-field survey that scans the northern sky to detect, characterize, and catalog photometric features of optical transients in the g , r , and i bands (referred to as zg , zr , and zi) using a custom-built mosaic camera mounted on the Samuel Oschin Telescope at Palomar Observatory and has been operational since 2018 (Bellm et al., 2019).

The data used in this work is part of the third ZTF data release (DR3), which includes approximately 9.4 months of observations from March to December 2018 (Masci et al., 2018). zr -band light curve data for 182 fields were selected from this release based on two quality cuts: (1) the object has at least 100 observations in the zr -band, and (2) the object quality is good according to ZTF pipeline⁵. ZTF object identifiers (OIDs), which are unique to each band and filter, are used to identify objects within these fields.

From these 182 fields, we selected a representative subset of 26 fields covering the ZTF footprint, as shown in Figure 1. To ensure a balanced selection, we first sorted the fields by the number of objects they contain and divided them into batches of seven. From each of the 26 batches, one field was randomly chosen. These selected fields were then analysed using the PINEFOREST anomaly detection algorithm (Section 4.1). The number of objects per field varies from 38, 623 to 9, 486, 393.

The light curve data for selected fields was processed using the *light-curve*⁶ package, a time-series feature extraction tool developed as part of the SNAD pipeline (Malanchev et al. 2021; Lavrukhina and Malanchev 2023). The extracted feature set consists of the same 42 zr -band features used in Pruzhinskaya et al. 2023.

3. Artefact labelling system

In Malanchev et al. 2021, 68% of the detected outliers were found to be bogus light curves that arise from detector/optical system, image subtraction issues, blending, and other effects. In this work, we group these bogus detections under the umbrella of ‘artefacts’ and try to isolate them in the feature-extracted light curve dataset.

To systematically label objects detected during our anomaly detection efforts, SNAD has developed its own tagging schema, which we follow in this work. The detailed definitions of the tags used in this dataset are provided in Section 3.1. This labelling system is self-consistent, designed to address SNAD specific challenges and requests, and may not fully align with classification schemes commonly used in the broader astronomical community.

We label only those artefacts that directly affect the central object and its photometry. Although different image defects can introduce additional artefacts within the cutout, we consider this approximation a reasonable starting point. Notably, the appearance of artefacts can vary depending on the cutout size – an artefact visible in a larger image may be absent in a smaller one. Introducing additional labels for non-central artefacts could lead to inconsistencies and misclassifications in the SNAD anomaly knowledge base. In order to maintain consistency and relevance across different tasks, we choose to label only the central object.

3.1. Types of artefacts

In the SNAD anomaly knowledge base, artefacts are categorized based on their origin, a requirement put in place to address the demands of the project and its collaborators. These form three broad groups of artefacts from the ZTF data: those originating from the detector, from the optical system, and those resulting from external factors (see Fig. 2).

³<https://snad.space>

⁴<https://coniferest.snad.space/>

⁵catflags=0 in ZTF DRs.

⁶<https://github.com/light-curve/light-curve-python>

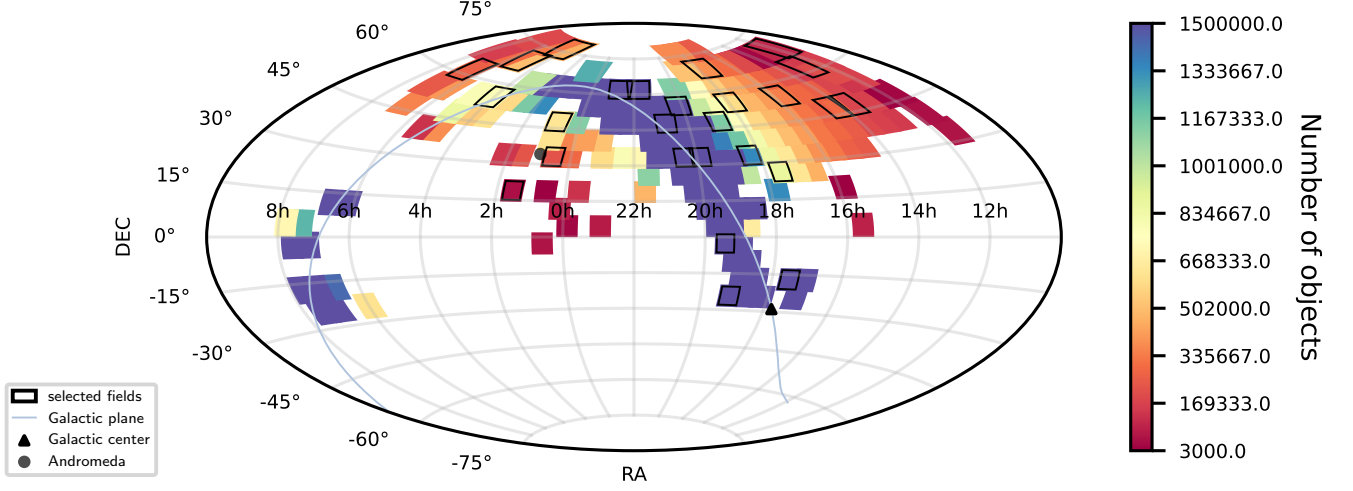


Figure 1: Distribution of the 182 feature-extracted fields from ZTF DR3 selected by applying the quality cuts mentioned in Section 2, color-coded by the number of objects in each. The black rectangles indicate the fields selected for this study.

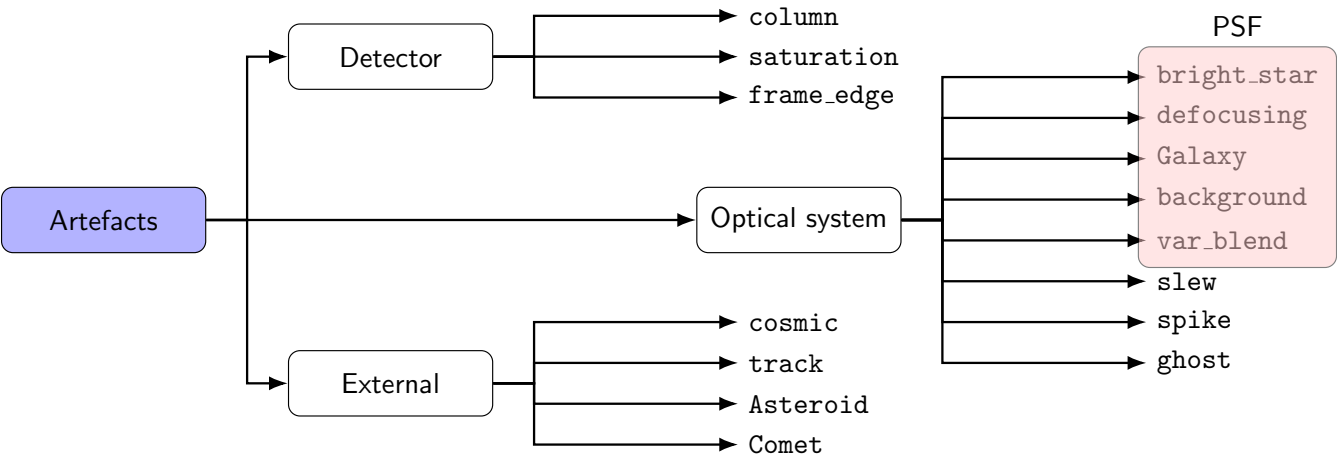


Figure 2: Figure showing the artefact labelling schema adopted in SNAD, as described in Section 3. All selected objects are tagged by the general label 'artefact' and then by the sub-labels according to their characteristics.

3.1.1. Detector artefacts

This category includes artefacts that arise from imperfections in the CCD detector. It contains the following tags:

- `column` describes bad pixel columns in the CCD that malfunction primarily due to production process issues. For example, some pixels do not turn on at all and stay dark/dead, while others always return hot/maximum signal. We also include traps under this category. Traps are damaged pixels that do not transfer the contained electrons properly when they are read out, causing partial data loss along the column.
- `saturation` occurs when a pixel exceeds its electron-holding capacity, leading to charge overflow into the neighboring pixels. It appears as a white streak or tail in images, and mostly occurs in very bright stars.
- `frame_edge` describes artefacts where a targeted object is located at the edge of the detector field of view.

3.1.2. Optical system artefacts

These artefacts are caused by the telescope’s optical system and are identified by the tags:

- `bright_star` refers to the proximity of an object whose scattered light contaminates the target and cannot be accurately subtracted.
- `defocusing` results from overlapping PSFs of nearby stars leading to blending or from optical defocusing.
- `Galaxy` denotes a galaxy being the primary target. In this case, PSF photometry is wrong since galaxies are not point sources. Moreover, most artefacts of this type also exhibit slight defocusing, further altering the PSF.
- `background` refers to irregular background gradients caused by improper sky subtraction.
- `var_blend` occurs when scattered-light echoes from nearby variable stars affect light curves of the primary target, introducing variability (see Section 6.2). The origin of this effect is the same as the `bright_star` artefact.
- `slew` refers to the patterns created as the telescope slews, i.e. when the mount is moved to point to a particular position in the sky. They often appear as long tails to bright stars or as criss-cross patterns in the image.
- `spike` refers to diffraction spikes caused by light bending around the support struts of the secondary mirror (spider), often seen around bright stars.
- `ghost` is a term used for internal reflection within lenses, filters and on its barrels. It comes in various shapes and sizes, the most common of which in our data is as a smudge around the targeted object.

3.1.3. External artefacts

External artefacts originate from sources outside the detector and optical system. The corresponding tags are:

- `cosmic` refers to cosmic rays striking the detector, which create single bright pixels or chains of bright pixels depending on the strike angle.
- `track` describes artefacts caused by aircraft or satellites crossing the field of view.
- `Asteroid` and `Comet` describe the cases when these celestial bodies overlap with the primary target, affecting its photometry.

4. Method

In this section, we describe the algorithms and methodologies used to create both the artefact and nominal datasets presented in this work.

4.1. PINEFOREST

PINEFOREST is an approach to active anomaly detection (AD) developed by the SNAD team, which has the widely used ISOLATION FOREST (Liu et al., 2008) algorithm as a foundation. ISOLATION FOREST is an AD spin on the decision tree method (Breiman 2001; Loh 2014; Hunt et al. 1966) which detects outliers under the assumption that anomalies are frequently isolated from the bulk of the data in large data sets. It is also the base algorithm in feedback-based (active) AD software currently in use in astronomy such as `coniferest` (Kornilov et al. 2024; Korolev et. al. in prep.) and `ASTRONOMALY` (Lochner and Bassett, 2021).

PINEFOREST was inspired by the ACTIVE ANOMALY DISCOVERY algorithm of Das et al. (2017). However instead of altering the basic structure of the trees, it discards altogether trees that quickly isolate objects which do not agree with the expert definition of anomaly. When a session is started in PINEFOREST, an initial ISOLATION FOREST is constructed using the input data. The user is then presented with the object that is assigned the highest outlier score and is prompted to determine whether it is ‘anomaly’ (scientifically interesting) or ‘regular’ (already known or not interesting for this study). If the user marks the object as an ‘anomaly’, the trees that assigned the status ‘regular’ to this object are discarded, new trees are grown in their place and the next iteration occurs.

In each step of the human-machine iteration loop, all labels collected so far are used to retrain the forest. The retraining process occurs in three stages: new trees are built on the original unlabeled dataset; both old and new trees are evaluated based on their ability to predict labeled data; trees with poor performance are removed, ensuring that the total number of trees remains the same as in the original forest. This iterative process of questions and filtering continues until a user-defined number of loops/budget are completed.

PINEFOREST is publicly available as a part of the `coniferest` suite along with the SNAD implementation of ISOLATION FOREST⁷ and the ACTIVE ANOMALY DISCOVERY algorithms.

⁷The `coniferest` version of ISOLATION FOREST is more efficient than the

4.2. Dataset of artefacts

As mentioned earlier, anomalies are a minority in any given dataset, making their random isolation time-consuming. This challenge motivates the use of an active anomaly detection algorithm, where prior decisions influence subsequent selections.

To that end, we run a PINEFOREST session with a budget of 50, selecting this many objects from each of the 26 chosen fields (1300 objects in total). Objects whose light curves exhibit atypical features corresponding to image artefacts (as defined in Section 3) are labelled as anomalies. The PINEFOREST parameters were set as follows: the number of trees to keep, n_trees , was 268, and the number of additional trees to be grown, n_spare_trees , was 768, with all other parameters set to default values.

The main output of a PINEFOREST session is a list of ZTF OIDs, anomaly scores, and user labels. To ensure labelling consistency, the detected anomalies were further inspected by a team of four experts. This review was conducted using SNAD ZTF Viewer⁸ (Malanchev et al., 2023), a web interface developed by the SNAD team that collates data, including light curves & FITS images for ZTF DRs, from multiple public databases where different aspects of the same object can be simultaneously inspected.

The final artefact dataset includes these curated objects, which have been labelled based on their light curves and corresponding image features.

4.3. Dataset of nominal objects

To highlight the differences between regular objects and artefacts, we also provide a nominal dataset containing the same number of objects as artefacts, selected from the same fields. These objects were randomly chosen from each field and verified as normal through a careful inspection of their light curves and FITS images from ZTF. Importantly, this dataset consists of images where no artefacts are present.

5. Results

Out of the 50 objects examined in each of the 26 selected ZTF fields, not all were artefacts as defined in Section 3. The exact number of images containing artefacts per ZTF field, along with the field’s central coordinates, is provided in Table 1. Examples of artefacts from different subtypes, along with their ZTF OIDs, are shown in Figure 3. The nominal dataset contains an equal number of normal objects selected from the same fields, with some examples shown in Figure 4.

In total, we labelled 1127 objects as artefacts with 1213 tags. The difference between the number of objects and the number of tags arises because, in some cases, a single object required up to three labels due to multiple effects occurring simultaneously. According to the classification defined in Section 3, the artefact

ZTF field	Centre coordinates in deg (ra, dec)	Number of artefacts/ nominals
284	287.22968, -24.25000	48
331	262.55696, -17.05000	50
437	291.41827, -2.65000	42
553	23.12473, 18.95000	36
635	263.32629, 26.15000	46
649	8.35811, 33.35000	46
683	274.70950, 33.35000	47
686	298.26936, 33.35000	49
687	306.08789, 33.35000	42
737	12.25000, 47.75000	45
757	204.72454, 47.75000	45
758	214.49923, 47.75000	33
765	282.92208, 47.75000	48
768	312.24615, 47.75000	43
778	60.11656, 54.95000	40
794	235.60357, 54.95000	39
797	268.89602, 54.95000	47
800	302.18847, 54.95000	47
813	100.00000, 62.15000	38
820	193.33333, 62.15000	45
830	326.66667, 62.15000	38
831	340.00000, 62.15000	40
837	77.14286, 69.35000	41
843	180.00000, 69.35000	37
848	265.71429, 69.35000	48
856	60.00000, 76.55000	47

Table 1: Summary of selected fields, including their central coordinates and the number of artefacts (also nominals) from each field included in the presented datasets.

dataset includes 265 detector artefact labels, 825 optical artefact labels, and 123 external artefact labels. Among the detector artefacts, the most common subtype is `column` (234), followed by `saturation` (25), while `frame_edge` (6) is the least common. The most frequent optical artefact label is `ghost` (391), making it the most common artefact overall. Among external artefacts, `track` (103) is the most frequent, while `cosmic` (4) is the least common, making it the rarest artefact label in the dataset. The detailed distribution of artefact subtypes is shown in Figure 5.

The final artefact dataset consists of 1127 images in FITS format, available in two sizes: 28×28 and 63×63 pixels. Table 2 lists the additional header entries included in the artefact FITS files, beyond those present in the original ZTF headers. The nominal dataset follows the same format, except for the absence of keyword entries. Both datasets, in both image sizes, are publicly available at Zenodo (<https://zenodo.org/records/15076426>).

6. Discussion

6.1. Distribution of artefacts by field

To investigate potential spatial dependencies in artefact distribution, we examined their occurrence in relation to field positions. We classified fields as ‘galactic’ (between -15 deg and $+15$ deg in galactic latitude) or ‘extragalactic’, and calculated the fraction of each artefact type in both groups (see Figure 5).

sklearn version and provides options for multithreading in processing. See Figure 1 and Section 4 in Kornilov et al. 2024 for a detailed comparison.

⁸<https://ztf.snad.space/>

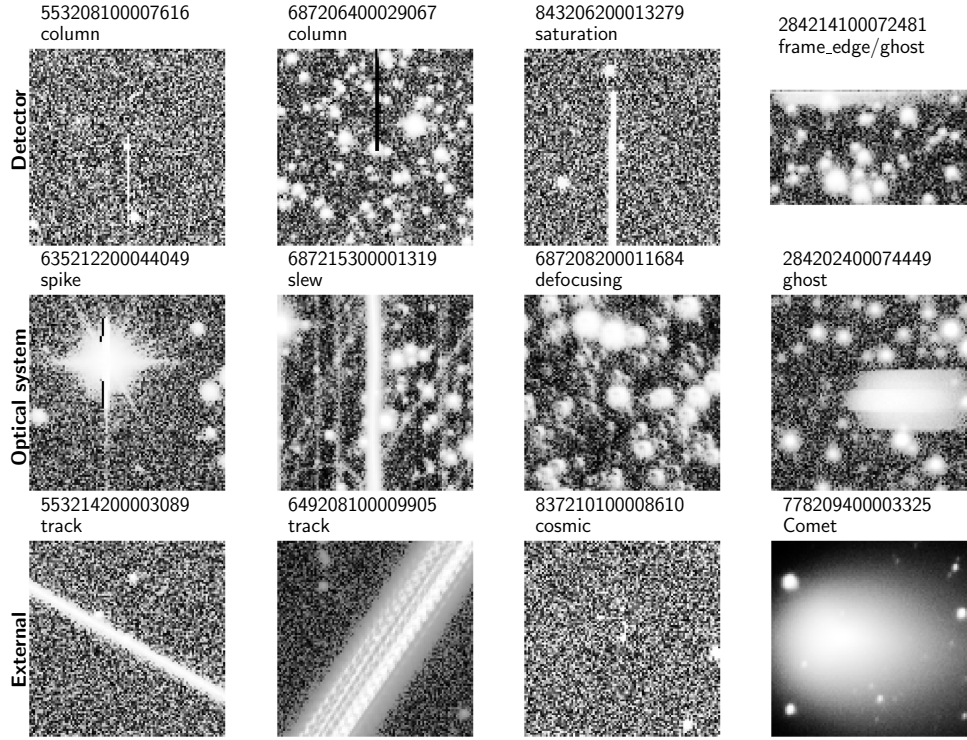


Figure 3: Figure showing examples of different types of artefacts isolated using PINEFOREST and labelled according to the schema defined in Section 3. The respective ZTF OIDs are displayed above each image cutout, along with their corresponding tags. The rows represent the three main label categories. The images are 100×100 pixels each in size and the astrometric directions follow the usual convention (North up, East left).

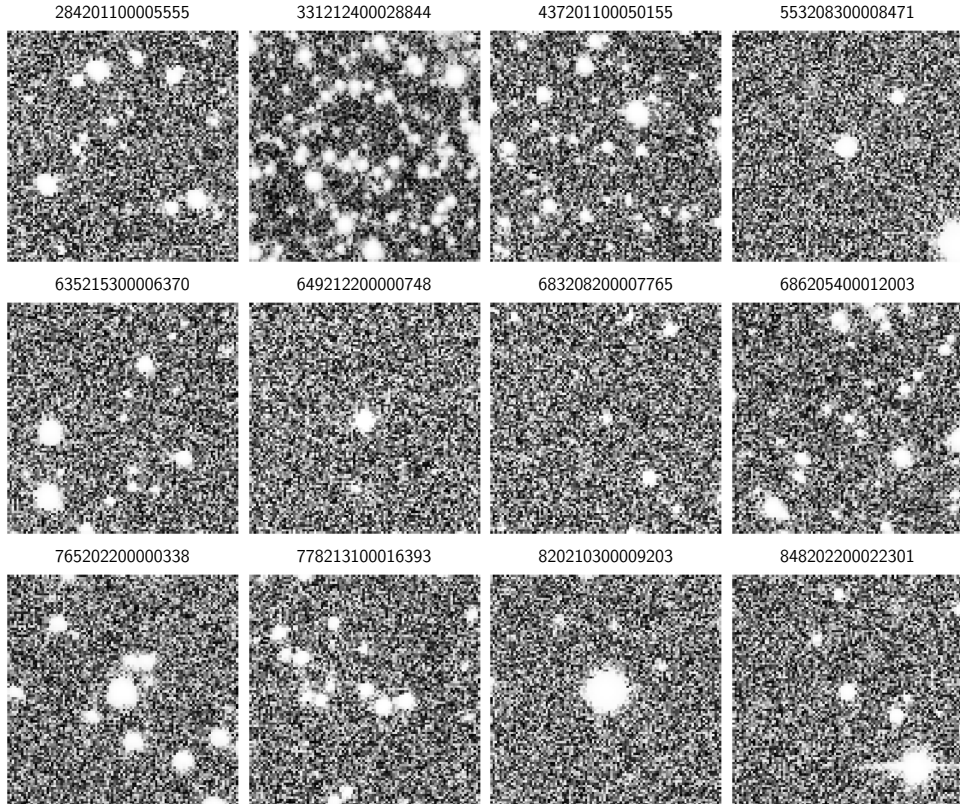


Figure 4: Figure showing some examples from the nominals dataset with their respective ZTF OIDs. The images are 100×100 pixels each in size and the astrometric directions follow the usual convention (North up, East left).

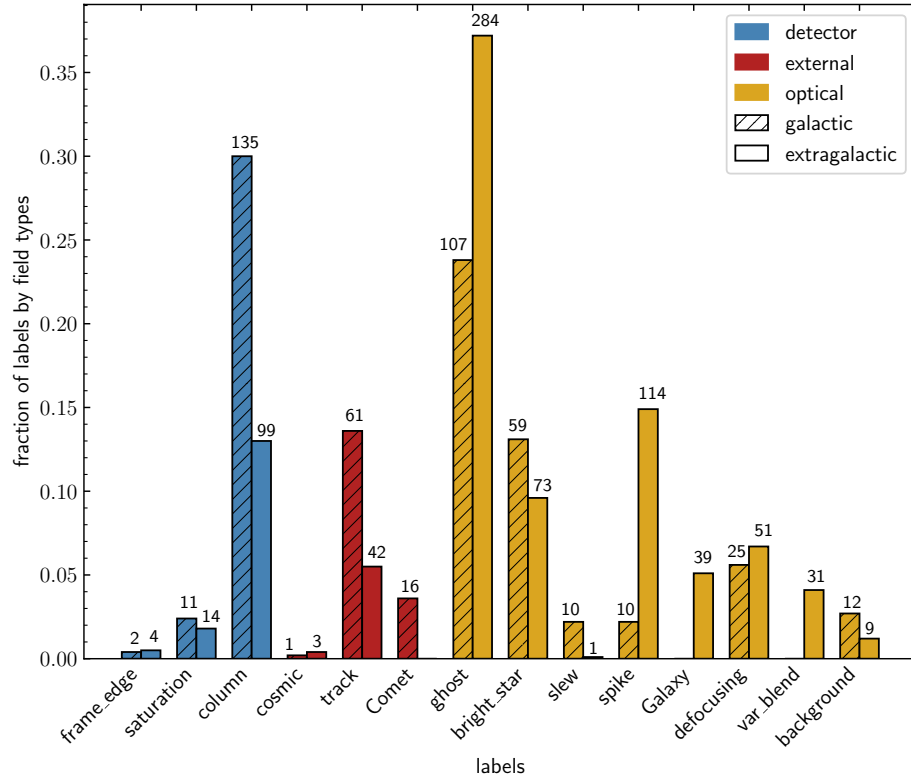


Figure 5: Bar plot showing the distribution of artefact labels in the dataset, separated into galactic and extragalactic fields. The x-axis lists the different artefact subtypes, while the y-axis represents their fraction within each group. The numbers above the bars indicate the total counts of each artefact type. The colour scheme follows the categorization of artefacts into detector-related (blue), external (red), and optical system (yellow) artefacts, as described in Section 3 and illustrated in Figure 2.

Keyword	Description
OID	ZTF object ID
OIDRA	Object Right Ascension (deg)
OIDDEC	Object Declination (deg)
TAGS	Labels for the central object according to the schema in Section 3.
URL	Download URL for the FITS image

Table 2: Table showing the additional entries that have been added to the ZTF FITS headers and their respective descriptions.

Some artefact types, such as `frame_edge`, `column`, and `ghost`, exhibit differences between galactic and extragalactic fields, but these variations are likely due to chance, as such artefacts originate from the CCD or system-related effects and do not depend on sky position. In contrast, bright-star-induced artefacts are expected to be more frequent in galactic fields, where the stellar density is higher. Indeed, this trend is evident for `bright_star` and `saturation`. However, interestingly, `spike` and `var_blend`, which are also linked to bright stars, are more common in extragalactic fields. The `Galaxy` tag, as expected, is found only in extragalactic fields, since background galaxies are largely obscured in the Galactic plane.

While these trends suggest potential spatial dependencies, the process of active anomaly detection introduces an additional layer of complexity. A key characteristic of active learning, and particularly of our active AD approach, is that each new decision made by the algorithm is influenced by prior interactions with an expert. This property may introduce a selection bias, affecting which artefacts are detected in certain fields and potentially masking true environmental or spatial dependencies. For example, if an expert labels an outlier as `ghost`, the algorithm is more likely to prioritize showing similar outliers in subsequent iterations. We observe this effect in some fields. For instance, in our dataset, every image in field 284 contains a `ghost` artefact. However, it is unclear whether this is due to selection bias or because ghosts are genuinely the most common artefact in that field. In contrast, field 553 exhibits a diverse range of artefacts.

6.2. Photometry of bright stars from artefact light curves

Some artefact light curves closely resemble those of real variable stars or transients, making it difficult to distinguish them from genuine astrophysical variability based on photometry alone. A key example is Mira-variable echoes, where light from a bright variable star contaminates a nearby source, creating the illusion of its variability. Figure 6 illustrates this effect. The top panel shows the zg - and zr -band light curves of the Mira variable TV Her, with its FITS image inset. The bottom panel presents a similar light curve and image for an object we labelled as `var_blend`. While the artefact light curve appears periodic, only the image reveals the true cause: contamination of nearby non-variable objects by light from a bright variable star (TV Her in this case). A similar issue occurs with `track` artefacts, where a single anomalous point in an otherwise normal light curve might resemble a transient event, such as a stellar

flare, until the image reveals it as a satellite track. This highlights the importance of combining light curve analysis with image inspection to correctly identify artefacts.

Moreover, `var_blend` artefacts offer an interesting scientific application. If a bright variable source is too saturated⁹ to be properly measured and is therefore absent from the survey data releases, its variability can still be inferred from the photometry of nearby contaminated sources. Consider the example of the Mira variable TV Her and its echos shown in Figure 6. Using the Lomb-Scargle periodogram (Lomb, 1976; Scargle, 1982), we estimated the period of the `var_blend` artefact (ZTF OID 683207400032110) to be 303.6 days, which is in remarkable agreement with the true period of TV Her (304.3 days¹⁰). This demonstrates that even artefact light curves can provide additional valuable astrophysical information about bright sources.

6.3. Interesting cases

6.3.1. Comet 21P/Giacobini-Zinner

We identified 16 instances of Comet 21P/Giacobini-Zinner within field 778 of our dataset. According to our labelling system, these are classified as external artefacts, as the distortion in the target light curve results from overlap with the comet’s light. Interestingly, such detections could serve as an indirect method for discovering new comets.

A video showing the motion of Comet 21P/Giacobini-Zinner from 2018-08-20 to 2018-09-20 can be viewed on the SNAD YouTube channel¹¹.

6.3.2. New eclipsing binary

During this work, we discovered a previously uncatalogued eclipsing binary with ZTF OID 831205400006945 (Fig. 7). The object has been added to the AAVSO VSX¹², the SNAD catalog¹³ and assigned the internal name SNAD260. Maximum and minimum magnitudes are 13.09^m and 13.73^m in zr -band, respectively. Its period, determined using the Lafler & Kinman method (Lafler and Kinman, 1965), is 23.7648 days.

7. Summary and conclusions

In this work, we present a dataset of artefacts detected in the Zwicky Transient Facility DR3 using the PINEFOREST active anomaly detection algorithm. We selected 26 ZTF fields, applied anomaly detection with a budget of 50 iterations per field, and labelled the detected artefacts following the SNAD classification schema. The final dataset consists of 1127 artefact

⁹According to the LSST Science Collaboration et al. 2009 estimates, saturation for a 15-second exposure in 0.7 arcsec seeing occurs at magnitudes of $u, g, r, i, z, y = 14.7^m, 15.7^m, 15.8^m, 15.8^m, 15.3^m$, and 13.9^m , respectively. Future large-scale surveys such as LSST are expected to contain a significant number of such cases.

¹⁰<https://www.aavso.org/vsx/index.php?view=detail.top&oid=14840>

¹¹<https://youtube.com/shorts/AZtcAL5e5fA?feature=shared>

¹²<https://www.aavso.org/vsx/index.php?view=detail.top&oid=10319899>

¹³<https://snad.space/catalog/>

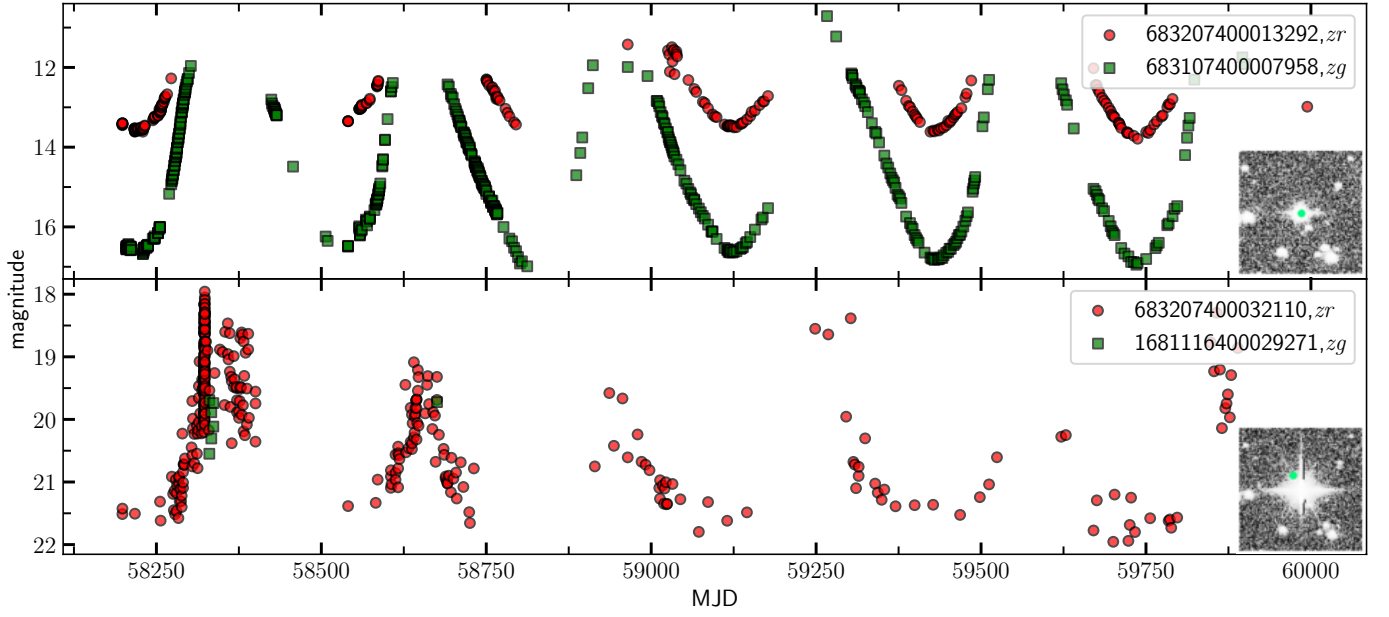


Figure 6: Illustration of the `var_blend` artefact label. The top panel shows the *zr* & *zg*-band light curves of a Mira variable (ZTF OID 683207400013292, also known as TV Her), with an inset showing its ZTF FITS image. The bottom panel shows the light curves of an object tagged as `var_blend` (ZTF OID 683207400032110), which represent scattered echoes of the same Mira variable in a different exposure. The inset images are 100×100 pixels in size, with a target marked by a green dot. Astrometric directions follow the standard convention (North up, East left).

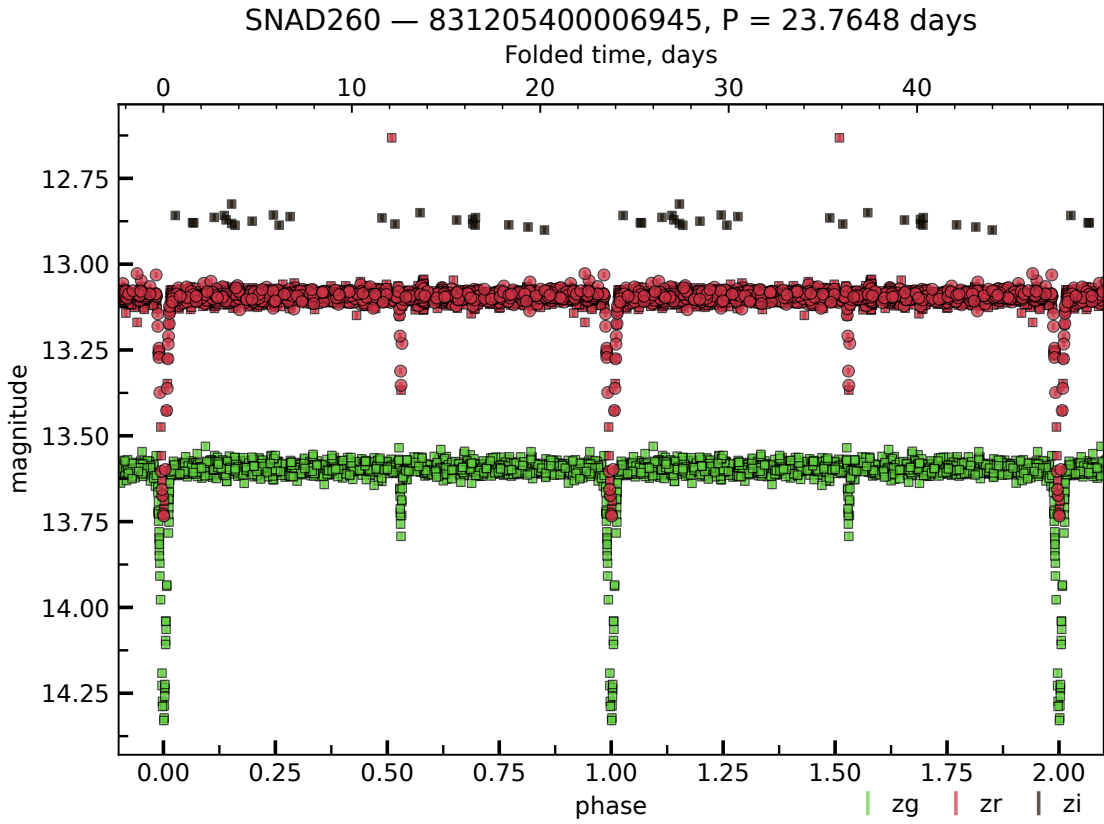


Figure 7: The folded light curves of eclipsing binary SNAD260. ZTF OIDs: 831205400006945, 831105400004328, 831305400076508, 1837114400010913, 1837214400022074, 832208300003915, 832108300002373.

images with a total of 1213 labels, as some objects exhibit multiple artefact types. Additionally, we provide a nominal dataset of 1127 nominal objects from the same fields for comparison. Both datasets are available in FITS format in two image sizes, 28×28 and 63×63 pixels.

The most common artefact type in our dataset is `ghost`, followed by `column` and `bright_star`, while the least frequent are `cosmic` and `frame_edge`. We investigated the spatial distribution of artefacts and found no clear correlation between artefact type and sky position. The classification of artefacts by active learning introduces an additional selection bias, as the algorithm prioritizes anomalies similar to those previously labelled by an expert.

In addition to the creation of the dataset of artefacts and nominal objects, we demonstrated a practical scientific application of artefact light curves. In particular, we showed that the variability period of a bright, saturated source can be recovered from the light curves of nearby contaminated objects. As an example, we measured the period of an artefact light curve contaminated by the light of a nearby Mira variable and found remarkable agreement with the true period of the Mira variable. We also reported the identification of 16 instances of Comet 21P/Giacobini-Zinner. This suggests that similar detections could provide an indirect method for identifying new comets. Finally, we discovered a previously uncatalogued eclipsing binary (ZTF OID 831205400006945), which has been added to the SNAD catalog under the designation SNAD260.

All astronomical surveys are affected by artefacts, making their automated identification and removal essential for maintaining high-quality catalogs. Machine learning approaches, particularly supervised learning methods, rely on labelled training data, which is often a limiting factor. While some studies use synthetic artefacts for training and citizen science initiatives such as Zooniverse, expert-labelled datasets remain a valuable resource for training and validating machine learning models. The datasets provided in this work can be used for real-bogus classification, anomaly detection, and survey catalog cleaning. Moreover, PINEFOREST active anomaly detection approach can be further adapted for targeted artefact identification in large surveys. Future applications may include LSST-era surveys, where the increasing volume of astronomical data will make automated artefact identification even more critical.

Acknowledgements

The study was conducted under the state assignment of Lomonosov Moscow State University. Support was provided by Schmidt Sciences, LLC. for K. Malanchev. The work of V. Krushinsky was supported by a project of youth scientific laboratory, topic FEUZ-2025-0003.

References

Bellm, E.C., Kulkarni, S.R., Graham, M.J., Dekany, R., Smith, R.M., Riddle, R., Masci, F.J., Helou, G., Prince, T.A., Adams, S.M., Barbarino, C., Barlow, T., Bauer, J., Beck, R., Belicki, J., Biswas, R., Blagorodnova, N.,

Bodewits, D., Bolin, B., Brinell, V., Brooke, T., Bue, B., Bulla, M., Burruss, R., Cenke, S.B., Chang, C.K., Connolly, A., Coughlin, M., Cromer, J., Cunningham, V., De, K., Delacroix, A., Desai, V., Duev, D.A., Eadie, G., Farnham, T.L., Feeney, M., Feindt, U., Flynn, D., Franckowiak, A., Frederick, S., Fremling, C., Gal-Yam, A., Gezari, S., Giomi, M., Goldstein, D.A., Golkhou, V.Z., Goobar, A., Groom, S., Hacopians, E., Hale, D., Henning, J., Ho, A.Y.Q., Hover, D., Howell, J., Hung, T., Huppenkothen, D., Imel, D., Ip, W.H., Ivezić, Ž., Jackson, E., Jones, L., Juric, M., Kasliwal, M.M., Kaspi, S., Kaye, S., Kelley, M.S.P., Kowalski, M., Kramer, E., Kupfer, T., Landry, W., Laher, R.R., Lee, C.D., Lin, H.W., Lin, Z.Y., Lunnan, R., Giomi, M., Mahabal, A., Mao, P., Miller, A.A., Monkewitz, S., Murphy, P., Ngeow, C.C., Nordin, J., Nugent, P., Ofek, E., Patterson, M.T., Penprase, B., Porter, M., Rauch, L., Rebbapragada, U., Reiley, D., Rigault, M., Rodriguez, H., van Roestel, J., Rusholme, B., van Santen, J., Schulze, S., Shupe, D.L., Singer, L.P., Soumagnac, M.T., Stein, R., Surace, J., Sollerman, J., Szkody, P., Taddia, F., Terek, S., Van Sistine, A., van Velzen, S., Vestrand, W.T., Walters, R., Ward, C., Ye, Q.Z., Yu, P.C., Yan, L., Zolkower, J., 2019. The Zwicky Transient Facility: System Overview, Performance, and First Results. *PASP* 131, 018002. doi:10.1088/1538-3873/aaecbe, arXiv:1902.01932.

Breiman, L., 2001. Random forests. *Machine learning* 45, 5–32.

Carrasco-Davis, R., Reyes, E., Valenzuela, C., Förster, F., Estévez, P.A., Pignata, G., Bauer, F.E., Reyes, I., Sánchez-Sáez, P., Cabrera-Vives, G., Eyheramendy, S., Catelan, M., Arredondo, J., Castillo-Navarrete, E., Rodríguez-Mancini, D., Ruz-Mieres, D., Moya, A., Sabatini-Gacitúa, L., Sepúlveda-Cobo, C., Mahabal, A.A., Silva-Farfán, J., Camacho-Iñiguez, E., Galbany, L., 2021. Alert Classification for the ALeRCE Broker System: The Real-time Stamp Classifier. *The Astronomical Journal* 162, 231. doi:10.3847/1538-3881/ac0ef1, arXiv:2008.03309.

Chang, C., Drlica-Wagner, A., Kent, S.M., Nord, B., Wang, D.M., Wang, M.H.L.S., 2021. A machine learning approach to the detection of ghosting and scattered light artifacts in dark energy survey images. *Astronomy and Computing* 36, 100474. doi:10.1016/j.ascom.2021.100474, arXiv:2105.10524.

Das, S., Wong, W.K., Fern, A., Dietterich, T.G., Siddiqui, M.A., 2017. Incorporating feedback into tree-based anomaly detection. arXiv preprint arXiv:1708.09441.

Desai, S., Mohr, J.J., Bertin, E., Kümmel, M., Wetzstein, M., 2016. Detection and removal of artifacts in astronomical images. *Astronomy and Computing* 16, 67–78. doi:10.1016/j.ascom.2016.04.002, arXiv:1601.07182.

Duev, D.A., Mahabal, A., Masci, F.J., Graham, M.J., Rusholme, B., Walters, R., Karmarkar, I., Frederick, S., Kasliwal, M.M., Rebbapragada, U., Ward, C., 2019. Real-bogus classification for the Zwicky Transient Facility using deep learning. *Monthly Notices of the Royal Astronomical Society* 489, 3582–3590. doi:10.1093/mnras/stz2357, arXiv:1907.11259.

Gardner, J.P., Mather, J.C., Clampin, M., Doyon, R., Greenhouse, M.A., Hammel, H.B., Hutchings, J.B., Jakobsen, P., Lilly, S.J., Long, K.S., Lunine, J.I., McCaughrean, M.J., Mountain, M., Nella, J., Rieke, G.H., Rieke, M.J., Rix, H.W., Smith, E.P., Sonneborn, G., Stiavelli, M., Stockman, H.S., Windhorst, R.A., Wright, G.S., 2006. The James Webb Space Telescope. *Space Sci. Rev.* 123, 485–606. doi:10.1007/s11214-006-8315-7, arXiv:astro-ph/0606175.

Hunt, E.B., Marin, J., Stone, P.J., 1966. Experiments in induction. Academic press.

Ishida, E.E.O., Kornilov, M.V., Malanchev, K.L., Pruzhinskaya, M.V., Volnova, A.A., Korolev, V.S., Mondon, F., Sreejith, S., Malancheva, A.A., Das, S., 2021. Active anomaly detection for time-domain discoveries. *aap* 650, A195. doi:10.1051/0004-6361/202037709, arXiv:1909.13260.

Ivezić, Ž., Kahn, S.M., Tyson, J.A., Abel, B., Acosta, E., Allsman, R., Alonso, D., AlSayyad, Y., Anderson, S.F., Andrew, J., Angel, J.R.P., Angeli, G.Z., Ansari, R., Antilogus, P., Araujo, C., Armstrong, R., Arndt, K.T., Astier, P., Aubourg, É., Auza, N., Axelrod, T.S., Bard, D.J., Barr, J.D., Barrau, A., Bartlett, J.G., Bauer, A.E., Bauman, B.J., Baumont, S., Bechtol, E., Bechtol, K., Becker, A.C., Becla, J., Beldica, C., Bellavia, S., Bianco, F.B., Biswas, R., Blanc, G., Blazek, J., Blandford, R.D., Bloom, J.S., Bogart, J., Bond, T.W., Booth, M.T., Borgland, A.W., Borne, K., Bosch, J.F., Boutigny, D., Brackett, C.A., Bradshaw, A., Brandt, W.N., Brown, M.E., Bullock, J.S., Burchat, P., Burke, D.L., Cagnoli, G., Calabrese, D., Callahan, S., Callen, A.L., Carlin, J.L., Carlson, E.L., Chandrasekharan, S., Charles-Emerson, G., Chesley, S., Cheu, E.C., Chiang, H.F., Chiang, J., Chirino, C., Chow, D., Ciardi, D.R., Claver, C.F., Cohen-Tanugi, J., Cockrum, J.J., Coles, R., Connolly, A.J., Cook, K.H., Cooray, A., Covey, K.R., Cribbs, C., Cui, W.,

- Cutri, R., Daly, P.N., Daniel, S.F., Daruich, F., Daubard, G., Daues, G., Dawson, W., Delgado, F., Dellapenna, A., de Peyster, R., de Val-Borro, M., Digel, S.W., Doherty, P., Dubois, R., Dubois-Felsmann, G.P., Durech, J., Economou, F., Eifler, T., Eracleous, M., Emmons, B.L., Fausti Neto, A., Ferguson, H., Figueroa, E., Fisher-Levine, M., Focke, W., Foss, M.D., Frank, J., Freemon, M.D., Gangler, E., Gawiser, E., Geary, J.C., Gee, P., Geha, M., Gessner, C.J.B., Gibson, R.R., Gilmore, D.K., Glanzman, T., Glick, W., Goldina, T., Goldstein, D.A., Goodenow, I., Graham, M.L., Gressler, W.J., Gris, P., Guy, L.P., Guyonnet, A., Haller, G., Harris, R., Hascall, P.A., Haupt, J., Hernandez, F., Herrmann, S., Hileman, E., Hoblitt, J., Hodgson, J.A., Hogan, C., Howard, J.D., Huang, D., Huffer, M.E., Ingraham, P., Innes, W.R., Jacoby, S.H., Jain, B., Jammes, F., Jee, M.J., Jenness, T., Jernigan, G., Jevremović, D., Johns, K., Johnson, A.S., Johnson, M.W.G., Jones, R.L., Juramy-Gilles, C., Jurić, M., Kalirai, J.S., Kallivayalil, N.J., Kalmbach, B., Kantor, J.P., Karst, P., Kasliwal, M.M., Kelly, H., Kessler, R., Kinnison, V., Kirkby, D., Knox, L., Kotov, I.V., Krabbendam, V.L., Krughoff, K.S., Kubánek, P., Kuczewski, J., Kulkarni, S., Ku, J., Kurita, N.R., Lage, C.S., Lambert, R., Lange, T., Langton, J.B., Le Guillou, L., Levine, D., Liang, M., Lim, K.T., Lintott, C.J., Long, K.E., Lopez, M., Lotz, P.J., Lupton, R.H., Lust, N.B., MacArthur, L.A., Mahabal, A., Mandelbaum, R., Markiewicz, T.W., Marsh, D.S., Marshall, P.J., Marshall, S., May, M., McKercher, R., McQueen, M., Meyers, J., Migliore, M., Miller, M., Mills, D.J., Miraval, C., Moeyens, J., Moolekamp, F.E., Monet, D.G., Moniez, M., Monkewitz, S., Montgomery, C., Morrison, C.B., Mueller, F., Muller, G.P., Muñoz Arancibia, F., Neill, D.R., Newbery, S.P., Nief, J.Y., Nomerotski, A., Nordby, M., O'Connor, P., Oliver, J., Olivier, S.S., Olsen, K., O'Mullane, W., Ortiz, S., Osier, S., Owen, R.E., Pain, R., Palecek, P.E., Parejko, J.K., Parsons, J.B., Pease, N.M., Peterson, J.M., Peterson, J.R., Petravick, D.L., Libby Petrick, M.E., Petry, C.E., Pierfederici, F., Pietrowicz, S., Pike, R., Pinto, P.A., Plante, R., Plate, S., Plutchak, J.P., Price, P.A., Prouza, M., Radeka, V., Rajagopal, J., Rasmussen, A.P., Regnault, N., Reil, K.A., Reiss, D.J., Reuter, M.A., Ridgway, S.T., Riot, V.J., Ritz, S., Robinson, S., Roby, W., Roodman, A., Rosing, W., Roucelle, C., Rumore, M.R., Russo, S., Saha, A., Sassolas, B., Schalk, T.L., Schellart, P., Schindler, R.H., Schmidt, S., Schneider, D.P., Schneider, M.D., Schoening, W., Schumacher, G., Schwamb, M.E., Sebag, J., Selvy, B., Sembroski, G.H., Seppala, L.G., Serio, A., Serrano, E., Shaw, R.A., Shipsey, I., Sick, J., Silvestri, N., Slater, C.T., Smith, J.A., Smith, R.C., Sobhani, S., Soldahl, C., Storrie-Lombardi, L., Stover, E., Strauss, M.A., Street, R.A., Stubbs, C.W., Sullivan, I.S., Sweeney, D., Swinbank, J.D., Szalay, A., Takacs, P., Tether, S.A., Thaler, J.J., Thayer, J.G., Thomas, S., Thornton, A.J., Thukral, V., Tice, J., Trilling, D.E., Turri, M., Van Berg, R., Vanden Berk, D., Vetter, K., Virieux, F., Vucina, T., Wahl, W., Walkowicz, L., Walsh, B., Walter, C.W., Wang, D.L., Wang, S.Y., Warner, M., Wiecha, O., Willman, B., Winters, S.E., Wittman, D., Wolff, S.C., Wood-Vasey, W.M., Wu, X., Xin, B., Yoachim, P., Zhan, H., 2019. LSST: From Science Drivers to Reference Design and Anticipated Data Products. *ApJ* 873, 111. doi:10.3847/1538-4357/ab042c, arXiv:0805.2366.
- Killestein, T.L., Lyman, J., Steeghs, D., Ackley, K., Dyer, M.J., Ulaczyk, K., Cutter, R., Mong, Y.L., Galloway, D.K., Dhillon, V., O'Brien, P., Ramsay, G., Poshayachinda, S., Kotak, R., Breton, R.P., Nuttall, L.K., Pallé, E., Pollacco, D., Thrane, E., Aukkaravittayapun, S., Awiphan, S., Burhanudin, U., Chote, P., Chrimes, A., Daw, E., Duffy, C., Eyles-Ferris, R., Gompertz, B., Heikkilä, T., Irawati, P., Kennedy, M.R., Levan, A., Littlefair, S., Makrygianni, L., Mata Sánchez, J., Mattila, S., Maund, J., McCormac, J., Mkrichian, D., Mullaney, J., Rol, E., Sawangwit, U., Stanway, E., Starling, R., Strøm, P.A., Tooke, S., Wiersema, K., Williams, S.C., 2021. Transient-optimized real-bogus classification with Bayesian convolutional neural networks - sifting the GOTO candidate stream. *Monthly Notices of the Royal Astronomical Society* 503, 4838–4854. doi:10.1093/mnras/stab633, arXiv:2102.09892.
- Kornilov, M.V., Korolev, V.S., Malanchev, K.L., Lavrukhina, A.D., Russeil, E., Semenikhin, T.A., Gangler, E., Ishida, E.E.O., Pruzhinskaya, M.V., Volnova, A.A., Sreejith, S., 2024. Coniferest: a complete active anomaly detection framework. URL: <https://arxiv.org/abs/2410.17142>, arXiv:2410.17142.
- Kornilov, V.G., Lipunov, V.M., Gorbvskoy, E.S., Belinski, A.A., Kuvshinov, D.A., Tyurina, N.V., Shatsky, N.I., Sankovich, A.V., Krylov, A.V., Balanutsa, P.V., Chazov, V.V., Kuznetsov, A.S., Zimnuhov, D.S., Senik, V.A., Tlatov, A.G., Parkhomenko, A.V., Dormidontov, D.V., Krushinsky, V.V., Zolozhnyh, I.S., Popov, A.A., Yazev, S.A., Budnev, N.M., Ivanov, K.I., Konstantinov, E.N., Gress, O.A., Chvalaev, O.V., Yurkov, V.V., Sergienko, Y.P., Kudelina, I.P., 2012. Robotic optical telescopes global network MASTER II. Equipment, structure, algorithms. *Experimental Astronomy* 33, 173–196. doi:10.1007/s10686-011-9280-z, arXiv:1111.6904.
- Laffer, J., Kinman, T.D., 1965. An RR Lyrae Star Survey with the Lick 20-INCH Astrograph II. The Calculation of RR Lyrae Periods by Electronic Computer. *ApJS* 11, 216. doi:10.1086/190116.
- Lavrukhina, A., Malanchev, K., 2023. Performant feature extraction for photometric time series. *Memorie della Società Astronomica Italiana Journal of the Italian Astronomical Society*, 102.
- Liu, F.T., Ting, K.M., Zhou, Z.H., 2008. Isolation forest, in: 2008 Eighth IEEE International Conference on Data Mining, pp. 413–422. doi:10.1109/ICDM.2008.17.
- Lochner, M., Bassett, B.A., 2021. ASTRONOMALY: Personalised active anomaly detection in astronomical data. *Astronomy and Computing* 36, 100481. doi:10.1016/j.ascom.2021.100481, arXiv:2010.11202.
- Loh, W.Y., 2014. Fifty years of classification and regression trees. *International Statistical Review* 82, 329–348.
- Lomb, N.R., 1976. Least-squares frequency analysis of unequally spaced data. *Astrophysics and space science* 39, 447–462.
- LSST Science Collaboration, Abell, P.A., Allison, J., Anderson, S.F., Andrew, J.R., Angel, J.R.P., Armus, L., Arnett, D., Asztalos, S.J., Axelrod, T.S., Bailey, S., Ballantyne, D.R., Bankert, J.R., Barkhouse, W.A., Barr, J.D., Barrientos, L.F., Barth, A.J., Bartlett, J.G., Becker, A.C., Becla, J., Beers, T.C., Bernstein, J.P., Biswas, R., Blanton, M.R., Bloom, J.S., Bochanski, J.J., Boeshaar, P., Borne, K.D., Bradac, M., Brandt, W.N., Bridge, C.R., Brown, M.E., Brunner, R.J., Bullock, J.S., Burgasser, A.J., Burge, J.H., Burke, D.L., Cargile, P.A., Chandrasekharan, S., Chartas, G., Chesley, S.R., Chu, Y.H., Cinabro, D., Claire, M.W., Claver, C.F., Clowe, D., Connolly, A.J., Cook, K.H., Cooke, J., Cooray, A., Covey, K.R., Culliton, C.S., de Jong, R., de Vries, W.H., Debattista, V.P., Delgado, F., Dell'Antonio, I.P., Dhital, S., Di Stefano, R., Dickinson, M., Dilday, B., Djorgovski, S.G., Dobler, G., Donalek, C., Dubois-Felsmann, G., Durech, J., Eliasdottir, A., Eracleous, M., Eyer, L., Falco, E.E., Fan, X., Fassnacht, C.D., Ferguson, H.C., Fernandez, Y.R., Fields, B.D., Finkbeiner, D., Figueroa, E.E., Fox, D.B., Francke, H., Frank, J.S., Frieman, J., Fromenteau, S., Furqan, M., Galaz, G., Gal-Yam, A., Garnavich, P., Gawiser, E., Geary, J., Gee, P., Gibson, R.R., Gilmore, K., Grace, E.A., Green, R.F., Gressler, W.J., Grillmair, C.J., Habib, S., Haggerty, J.S., Hamuy, M., Harris, A.W., Hawley, S.L., Heavens, A.F., Hebb, L., Henry, T.J., Hileman, E., Hilton, E.J., Hoadley, K., Holberg, J.B., Holman, M.J., Howell, S.B., Infante, L., Ivezić, Z., Jacoby, S.H., Jain, B., Jedicke, J., Jee, M.J., Garrett Jernigan, J., Jha, S.W., Johnston, K.V., Jones, R.L., Juric, M., Kaasalainen, M., Styliani, Kafka, Kahn, S.M., Kaib, N.A., Kalirai, J., Kantor, J., Kasliwal, M.M., Keeton, C.R., Kessler, R., Knezevic, Z., Kowalski, A., Krabbendam, V.L., Krughoff, K.S., Kulkarni, S., Kuhlman, S., Lacy, M., Lepine, S., Liang, M., Lien, A., Lira, P., Long, K.S., Lorenz, S., Lotz, J.M., Lupton, R.H., Lutz, J., Macri, L.M., Mahabal, A.A., Mandelbaum, R., Marshall, P., May, M., McGehee, P.M., Meadows, B.T., Meert, A., Milani, A., Miller, C.J., Miller, M., Mills, D., Minniti, D., Monet, D., Mukadam, A.S., Nakar, E., Neill, D.R., Newman, J.A., Nikolaev, S., Nordby, M., O'Connor, P., Oguri, M., Oliver, J., Olivier, S.S., Olsen, J.K., Olsen, K., Olszewski, E.W., Oluseyi, H., Padilla, N.D., Parker, A., Pepper, J., Peterson, J.R., Petry, C., Pinto, P.A., Pizagno, J.L., Popescu, B., Prsa, A., Radcka, V., Raddick, M.J., Rasmussen, A., Rau, A., Rho, J., Rhoads, J.E., Richards, G.T., Ridgway, S.T., Robertson, B.E., Roskar, R., Saha, A., Sarajedini, A., Scannapieco, E., Schalk, T., Schindler, R., Schmidt, S., 2009. LSST Science Book, Version 2.0. arXiv e-prints, arXiv:0912.0201doi:10.48550/arXiv.0912.0201, arXiv:0912.0201.
- Malanchev, K., Kornilov, M.V., Pruzhinskaya, M.V., Ishida, E.E.O., Aleo, P.D., Korolev, V.S., Lavrukhina, A., Russeil, E., Sreejith, S., Volnova, A.A., Voloshina, A., Krone-Martins, A., 2023. The SNAD Viewer: Everything You Want to Know about Your Favorite ZTF Object. *pasp* 135, 024503. doi:10.1088/1538-3873/acb292, arXiv:2211.07605.
- Malanchev, K., Pruzhinskaya, M., Korolev, V., Aleo, P., Kornilov, M., Ishida, E., Krushinsky, V., Mondon, F., Sreejith, S., Volnova, A., et al., 2021. Anomaly detection in the zwicky transient facility dr3. *Monthly Notices of the Royal Astronomical Society* 502, 5147–5175.
- Masci, F.J., Laher, R.R., Rusholme, B., Shupe, D.L., Groom, S., Surace, J., Jackson, E., Monkewitz, S., Beck, R., Flynn, D., Terek, S., Landry, W., Hecopians, E., Desai, V., Howell, J., Brooke, T., Imel, D., Wachter, S., Ye, Q.Z., Lin, H.W., Cenko, S.B., Cunningham, V., Rebbapragada, U., Bue, B., Miller, A.A., Mahabal, A., Bellm, E.C., Patterson, M.T., Jurić, M., Golkhou,

- V.Z., Ofek, E.O., Walters, R., Graham, M., Kasliwal, M.M., Dekany, R.G., Kupfer, T., Burdge, K., Cannella, C.B., Barlow, T., Sistine, A.V., Giomi, M., Fremling, C., Blagorodnova, N., Levitan, D., Riddle, R., Smith, R.M., Helou, G., Prince, T.A., Kulkarni, S.R., 2018. The zwicky transient facility: Data processing, products, and archive. Publications of the Astronomical Society of the Pacific 131, 018003. URL: <https://dx.doi.org/10.1088/1538-3873/aae8ac>, doi:10.1088/1538-3873/aae8ac.
- Paranjpye, D., Mahabal, A., Ramaprakash, A.N., Panopoulou, G.V., Cleary, K., Readhead, A.C.S., Blinov, D., Tassis, K., 2019. Eliminating artefacts in polarimetric images using deep learning. Monthly Notices of the Royal Astronomical Society 491, 5151–5157. URL: <https://doi.org/10.1093/mnras/stz3250>, doi:10.1093/mnras/stz3250, arXiv:<https://academic.oup.com/mnras/article-pdf/491/4/5151/31608743>.
- Pöntinen, M., Granvik, M., Nucita, A.A., Conversi, L., Altieri, B., Carry, B., O’Riordan, C.M., Scott, D., Aghanim, N., Amara, A., Amendola, L., Aurichio, N., Baldi, M., Bonino, D., Branchini, E., Brescia, M., Camera, S., Capobianco, V., Carbone, C., Carretero, J., Castellano, M., Cavuoti, S., Cimatti, A., Cledassou, R., Congedo, G., Copin, Y., Corcione, L., Courbin, F., Cropper, M., Da Silva, A., Degaudenzi, H., Dinis, J., Dubath, F., Dupac, X., Dusini, S., Farrens, S., Ferriol, S., Frailis, M., Franceschi, E., Fumana, M., Galeotta, S., Garilli, B., Gillard, W., Gillis, B., Giocoli, C., Grazian, A., Haugan, S.V.H., Holmes, W., Hornuth, F., Hornstrup, A., Jahnke, K., Kümmel, M., Kermiche, S., Kiessling, A., Kitching, T., Kohley, R., Kunz, M., Kurki-Suonio, H., Ligor, S., Lilje, P.B., Lloro, I., Maiorano, E., Mansutti, O., Marggraf, O., Markovic, K., Marulli, F., Massey, R., Medinaceli, E., Mei, S., Melchior, M., Mellier, Y., Meneghetti, M., Meylan, G., Moresco, M., Moscardini, L., Munari, E., Niemi, S.M., Nutma, T., Padilla, C., Paltani, S., Pasian, F., Pedersen, K., Pettorino, V., Pires, S., Polenta, G., Poncet, M., Raison, F., Renzi, A., Rhodes, J., Riccio, G., Romelli, E., Roncarelli, M., Rossetti, E., Saglia, R., Sapone, D., Sartoris, B., Schneider, P., Secroun, A., Seidel, G., Serrano, S., Sirignano, C., Sirri, G., Stanco, L., Tallada-Crespí, P., Taylor, A.N., Tereno, I., Toledo-Moreo, R., Torradeflot, F., Tutusaus, I., Valenziano, L., Vassallo, T., Verdoes Kleijn, G., Wang, Y., Weller, J., Zamorani, G., Zoubian, J., Scottez, V., 2023. Euclid: Identification of asteroid streaks in simulated images using deep learning. A&A 679, A135. doi:10.1051/0004-6361/202347551, arXiv:2310.03845.
- Pruzhinskaya, M.V., Ishida, E.E.O., Novinskaya, A.K., Russeil, E., Volnova, A.A., Malanchev, K.L., Kornilov, M.V., Aleo, P.D., Korolev, V.S., Krushinsky, V.V., Sreejith, S., Gangler, E., 2023. Supernova search with active learning in ZTF DR3. aap 672, A111. doi:10.1051/0004-6361/202245172, arXiv:2208.09053.
- Pruzhinskaya, M.V., Malanchev, K.L., Kornilov, M.V., Ishida, E.E., Mondon, F., Volnova, A.A., Korolev, V.S., 2019. Anomaly detection in the open supernova catalog. Monthly Notices of the Royal Astronomical Society 489, 3591–3608.
- Refregier, A., Amara, A., Kitching, T.D., Rassat, A., Scaramella, R., Weller, J., 2010. Euclid Imaging Consortium Science Book. arXiv e-prints , arXiv:1001.0061arXiv:1001.0061.
- Sánchez-Sáez, P., Lira, H., Martí, L., Sánchez-Pi, N., Arredondo, J., Bauer, F.E., Bayo, A., Cabrera-Vives, G., Donoso-Oliva, C., Estévez, P.A., Eyheramendy, S., Förster, F., Hernández-García, L., Arancibia, A.M.M., Pérez-Carrasco, M., Sepúlveda, M., Vergara, J.R., 2021. Searching for Changing-state AGNs in Massive Data Sets. I. Applying Deep Learning and Anomaly-detection Techniques to Find AGNs with Anomalous Variability Behaviors. AJ 162, 206. doi:10.3847/1538-3881/ac1426, arXiv:2106.07660.
- Sankar, R., Brueshaber, S., Fortson, L., Hansen-Koharcheck, C., Lintott, C., Mantha, K., Nesmith, C., Orton, G.S., 2024. Jovian vortex hunter: A citizen science project to study jupiter’s vortices. The Planetary Science Journal 5, 203. URL: <https://dx.doi.org/10.3847/PSJ/ad6e75>, doi:10.3847/PSJ/ad6e75.
- Scargle, J.D., 1982. Studies in astronomical time series analysis. ii-statistical aspects of spectral analysis of unevenly spaced data. Astrophysical Journal, Part 1, vol. 263, Dec. 15, 1982, p. 835-853. 263, 835–853.
- Semenikhin, T.A., Kornilov, M.V., Pruzhinskaya, M.V., Lavrukhina, A.D., Russeil, E., Gangler, E., Ishida, E.E.O., Korolev, V.S., Malanchev, K.L., Volnova, A.A., Sreejith, S., 2024. Real-bogus scores for active anomaly detection. arXiv e-prints , arXiv:2409.10256doi:10.48550/arXiv.2409.10256, arXiv:2409.10256.
- Tanoglidis, D., Čiprijanović, A., Drlica-Wagner, A., Nord, B., Wang, M.H.L.S., Amsellem, A.J., Downey, K., Jenkins, S., Kafkes, D., Zhang, Z., 2022. DeepGhostBusters: Using Mask R-CNN to detect and mask ghosting and scattered-light artifacts from optical survey images. Astronomy and Computing 39, 100580. doi:10.1016/j.ascom.2022.100580, arXiv:2109.08246.
- Volnova, A.A., Aleo, P.D., Lavrukhina, A., Russeil, E., Semenikhin, T., Gangler, E., Ishida, E.E.O., Kornilov, M.V., Korolev, V., Malanchev, K., Pruzhinskaya, M.V., Sreejith, S., 2024. Exploring the universe with snad: Anomaly detection in astronomy, in: Baixerries, J., Ignatov, D.I., Kuznetsov, S.O., Stupnikov, S. (Eds.), Data Analytics and Management in Data Intensive Domains, Springer Nature Switzerland, Cham. pp. 195–208.
- Voloshina, A.S., Lavrukhina, A.D., Pruzhinskaya, M.V., Malanchev, K.L., Ishida, E.E.O., Krushinsky, V.V., Aleo, P.D., Gangler, E., Kornilov, M.V., Korolev, V.S., Russeil, E., Semenikhin, T.A., Sreejith, S., Volnova, A.A., 2024. SNAD catalogue of M-dwarf flares from the Zwicky Transient Facility. Monthly Notices of the Royal Astronomical Society 533, 4309–4323. doi:10.1093/mnras/stae2031, arXiv:2404.07812.
- Weston, J.G., Smith, K.W., Smartt, S.J., Tonry, J.L., Stevance, H.F., 2024. Training a convolutional neural network for real-bogus classification in the ATLAS survey. RAS Techniques and Instruments 3, 385–399. URL: <https://doi.org/10.1093/rasti/rzae027>, doi:10.1093/rasti/rzae027, arXiv:<https://academic.oup.com/rasti/article-pdf/3/1/385/58738311/>